ANNALS of Faculty Engineering Hunedoara – International Journal of Engineering
Tome XVIII [2020] | Fascicule 2 [May]

ANNALS of Faculty Engineering Hunedoara – International Journal of Engineering
ISSN 1584-2665 (printed version); ISSN 2601-2332 (online); ISSN-L 1584-2665

[1.]Dimbeswar KALITA, [1.]Silpi HAZARIKA, [2.]Sahin AHMED

MHD DRAG FORCE ON WATER BASED CYLINDRICAL SHAPED ZnO NANOPARTICLE IN A CHEMICALLY REACTING NANOFLUID THROUGH CHANNEL: A THEORETICAL INVESTIGATION

[1.]Department of Mathematics, Mangaldai College, Assam, INDIA
[2.]Department of Mathematics, Rajiv Gandhi University, Itangar, Arunachal Pradesh, INDIA

Abstract: An electrically conducting hydromagnetic flow of Cylindrical shaped Zinc Oxide (ZnO) and water based nanofluid is taken to investigate theoretically the behavior of various key parameter like magnetic field, heat generation, porosity, radiation and first order chemical reaction on velocity, temperature and concentration equations in a vertical channel embedded with saturated porous medium. The analytical solutions of the equations are obtained and the impact of the controlling parameters on the velocity, temperature, concentration, skin friction, Nusselt number and Sherwood number has been discussed graphically. It is concluded that with increase of ϕ, both the velocity and temperature diminish. Moreover, the magnetic parameter retards the nanofluid motion whereas porosity accelerates it. Due to the presence of ZnO, the shear stresses become negative throughout the channel of porous medium. ZnO nanoparticles have used worldwide for their exclusive advances in biomedical applications (cancer cell imaging, sun screens), toxicity study, textiles and hybrid solar cells etc.
Keywords: ZnO-water based nanofluid, Nanoparticles volume fractions, Permeability parameter, Mass Transfer, Channel flow

1. INTRODUCTION

The idea of utilizing nanoparticles (alumina (Al_2O_3), Zinc oxide (ZnO), Copper (Cu), Silver (Ag) etc.) by adding limited quantity of nanoparticles to the base fluid (water, ethylene glycol, engine oil, grease oils etc.), which have poor thermal conductivity contrasted with that of solid nanoparticles is initiated by Choi in 1995. The pioneer work of remarkable increments in the thermal conductivity of Nanofluids, they have become the topic of lots of research. In 21st century due to the improved properties related with mass and heat transfer, anti-bacterial wetting, and spreading action, much research has been done on nanofluids. Potential uses of nanofluids incorporate transportation, cooling process like to cool automobile engines and high heat flux devices (microwave tubes etc), biomedicine, refrigeration, energy industry and so on. Now a day's ZnO is one of the most prominent metal oxide nanoparticles used in recent Nanotechnology due to its peculiar physical and chemical properties and has driven attention towards research.

Nanofluids play an important role to upgrade the heat transfer execution contrasted with pure or base fluids, so they can be considered as the most energizing heat transfer fluids. Further some detail latest exploration on nanofluid of different nanoparticles with various properties is attempted by several researchers in References (2016, 2018, 2017, 2016, 2017). Enhancement of heat transfer characteristics in the channel with trapezoidal rib–groove using nanofluids is studied by Al-Shamani et al. (2015). Hayat et al. (2015) discussed the mixed convection flow of Casson nanofluid over a stretching sheet with convectively heated chemical reaction and heat Source/Sink. Aaiza et al. (2015) observed the energy transfer in mixed convection MHD flow of nanofluid containing different shapes of nanoparticles in a channel filled with saturated porous medium.

There have been numerous investigations (2015, 2013, 2013, 2015, 2018) on the nanofluid with various effects such as heat transfer, thermal conductivity, MHD, thermal radiations, porous medium and so on. Pandey et.al (2017) studied the chemical reaction and thermal radiation effects on boundary layer flow of nanofluid over a wedge with viscous and Ohmic dissipation. MHD flow and radiation heat transfer of nanofluids in porous media with variable surface and chemical reaction is discussed by Zhang et al. (2015).Heat and mass transfer study of nanofluid with various effect is investigated by many researchers in recent years (2016, 2016). Prateek et al. (2016) reviewed the applications and properties of Zinc Oxide (Zno) nanoparticles. Recently, Dogonchi et al. (2017) studied the MHD Go-water nanofluid flow and heat transfer in a porous channel in the presence of thermal radiation effect.

This study is aimed to investigate the mixed convection MHD flow of cylindrical shape ZnO nanoparticles in water based nanofluid in a vertical permeable channel in presence of heat generation, thermal radiation and first order chemical reaction. The effects of key parameters like MHD drag force, Radiation, Chemical reaction and nanoparticle volume fraction on velocity, temperature and concentration are discussed and presented graphically as well as discussed the behaviour of skin friction, Nusselt number and Sherwood number.

2. MATHEMATICAL FORMULATION

The $\bar{\mathbf{x}}$– axis is taken along the flow and $\bar{\mathbf{y}}$– axis is taken normal to the flow direction. The mixed convection is caused due to buoyancy force together with external pressure gradient applied along the $\bar{\mathbf{x}}$– direction. Under the usual assumption of Boussinesq approximation, the governing equations of momentum, energy and mass are as follow:

$$\rho_{nf}\frac{\partial \bar{u}}{\partial \bar{t}} = -\frac{\partial \bar{p}}{\partial \bar{x}} + \mu_{nf}\frac{\partial^2 \bar{u}}{\partial \bar{y}^2} + (\rho\beta)_{nf} g\left(\bar{T}-\bar{T}_0\right) + (\rho\beta)_{nf} g\left(\bar{C}-\bar{C}_0\right) - \left(\sigma B_0^2 + \frac{\mu_{nf}}{\bar{K}_1}\right)\bar{u}, \qquad (2.1)$$

$$\left(\rho C_p\right)_{nf}\frac{\partial \bar{T}}{\partial \bar{t}} = \kappa_{nf}\frac{\partial^2 \bar{T}}{\partial \bar{y}^2} - \frac{\partial \bar{q}}{\partial \bar{y}} - Q_0\left(\bar{T}-\bar{T}_0\right), \qquad (2.2)$$

$$\left(\frac{\partial \bar{C}}{\partial \bar{t}} + \bar{v}\frac{\partial \bar{C}}{\partial \bar{y}}\right) = D_B\frac{\partial^2 \bar{C}}{\partial \bar{y}^2} - K_l(\bar{C}-\bar{C}_0) . \qquad (2.3)$$

In order to encounter spherical shape of nanoparticles inside nanofluids, Hamilton and Crosser (1962) model for thermal conductivity and the Timofeeva et al. (2009) model for calculating dynamic viscosity of nanofluids have been used and they are:

$$\left\{\begin{array}{c} n = \dfrac{3}{\psi}, \quad \mu_{nf} = \mu_f(1 + a\phi + b\phi^2), \quad (\rho)_{nf} = (1-\phi)(\rho)_f + \phi(\rho)_s, \\ (\rho\beta)_{nf} = (1-\phi)(\rho\beta)_f + \phi(\rho\beta)_s, \quad \left(\rho C_p\right)_{nf} = (1-\phi)\left(\rho C_p\right)_f + \phi\left(\rho C_p\right)_s, \\ \dfrac{\kappa_{nf}}{\kappa_f} = \dfrac{\kappa_s + (n-1)\kappa_f + (n-1)(\kappa_s-\kappa_f)\phi}{\kappa_s + (n-1)\kappa_f - (\kappa_s-\kappa_f)\phi}, \sigma_{nf} = \sigma_f\left[1 + \dfrac{3(\sigma-1)\phi}{(\sigma+2)-(\sigma-1)\phi}\right] \end{array}\right\} \qquad (2.4)$$

The radiative heat flux is given by,

$$\frac{\partial \bar{q}}{\partial \bar{y}} = -4\alpha^2\left(\bar{T}-\bar{T}_0\right) \qquad (2.5)$$

The nondimensional parameters are:

$$\left\{\begin{array}{c} x = \dfrac{\bar{x}}{d}, \; y = \dfrac{\bar{y}}{d}, \; u = \dfrac{\bar{u}}{U_0}, \; t = \dfrac{\bar{t}U_0}{d}, \; \nu_f = \dfrac{\mu_f}{\rho_f}, \; K = \dfrac{\bar{K}_1}{d^2}, \; \lambda_n = \dfrac{\kappa_{nf}}{\kappa_f}, \\ \theta = \dfrac{\bar{T}-\bar{T}_0}{\bar{T}_w-\bar{T}_0}, C = \dfrac{\bar{C}-\bar{C}_0}{\bar{C}_w-\bar{C}_0} \; p = \dfrac{\bar{p}d}{\mu\, U_0}, \; \omega = \dfrac{\bar{\omega}d}{U_0}, \; \dfrac{\partial p}{\partial x} = \lambda\exp(i\omega t), \\ Pe = \dfrac{U_0 d(\rho C_p)_f}{k_f}, Re = \dfrac{U_0 d}{\nu_f}, \; M^2 = \dfrac{\sigma d^2 B_0^2}{\mu_f}, \\ Gr = \dfrac{d^2 g\beta_f(T_w-T_0)}{U_0\mu_f}, Gm = \dfrac{d^2 g\beta_f(\bar{C}_w-\bar{C}_0)}{U_0\mu_f}, \\ R^2 = \dfrac{4d^2\alpha^2}{\kappa_f}, \; Q = \dfrac{d^2 Q_0}{\kappa_{nf}}, S = \dfrac{V_0}{U_0}, Sc = \dfrac{U_0 d}{D_B}, Kr = \dfrac{K_l d}{U_0} \end{array}\right\} \qquad (2.6)$$

With the help of (2.4) – (2.6), the eqs (2.1) – (2.3) reduce to the dimensionless form

$$\phi_1 Re\frac{\partial u}{\partial t} = \varepsilon\lambda \exp(i\omega t) + \phi_2\frac{\partial^2 u}{\partial y^2} - M^2 u - \frac{\phi_2}{K}u + \phi_3 Gr\theta \tag{2.7}$$

$$\phi_4 Pe\frac{1}{\lambda_n}\frac{\partial\theta}{\partial t} = \frac{\partial^2\theta}{\partial y^2} + \frac{R^2}{\lambda_n}\theta - Q\theta \tag{2.8}$$

$$\frac{\partial C}{\partial t} - S\frac{\partial C}{\partial y} = \frac{1}{Sc}\frac{\partial^2 C}{\partial y^2} - KrC \tag{2.9}$$

The boundary conditions are

$$\begin{Bmatrix} \bar{u}(0,t) = 0, & \bar{u}(d,t) = 0 \\ \bar{T}(0,t) = T_0, & \bar{T}(d,t) = T_\infty \\ \bar{C}(0,t) = C_0, & \bar{C}(d,t) = C_\infty \end{Bmatrix} \tag{2.10 }$$

The dimensionless forms of (2.10) are

$$\begin{Bmatrix} u(0,t) = 0, & u(1,t) = 0, & t > 0 \\ \theta(0,t) = 0, & \theta(1,t) = 1, & t > 0 \\ C(0,t) = 0, & C(1,t) = 1, & t > 0 \end{Bmatrix} \tag{2.11}$$

The eqs (2.7) and (2.9) may be re-written as

$$a_0\frac{\partial u}{\partial t} = \varepsilon\lambda \exp(i\omega t) + \phi_2\frac{\partial^2 u}{\partial y^2} - m_0^2 u + a_1\theta \tag{2.12}$$

$$b_0^2\frac{\partial\theta}{\partial t} = \frac{\partial^2\theta}{\partial y^2} + (b_1^2 - Q)\theta \tag{2.13}$$

$$\frac{\partial C}{\partial t} - S\frac{\partial C}{\partial y} = \frac{1}{Sc}\frac{\partial^2 C}{\partial y^2} - KrC \tag{2.14}$$

To solve the eqs (2.12) - (2.13) with the boundary conditions (2.11), the perturbed solutions are taken of the forms:

$$f(y,t) = f_0(y) + \varepsilon \exp(i\omega t) f_1(y) \tag{2.15}$$

where f stands for u, θ or C.

On using the eqs (2.15) into eqs (2.12) - (2.14), we obtain the following system of ordinary differential equations,

$$\frac{d^2 u_0(y)}{dy^2} - m_1^2 u_0(y) = -a_3\theta_0(y) - -a_4 C_0(y), \tag{2.16}$$

$$\frac{d^2 u_1(y)}{dy^2} - m_2^2 u_1(y) = -\lambda_1 - a_3\theta_1(y) - -a_4 C_1(y)\,, \tag{2.17}$$

$$\frac{d^2\theta_0(y)}{dy^2} + b_2^2\theta_0(y) = 0\,, \tag{2.18}$$

$$\frac{d^2\theta_1(y)}{dy^2} + b_3^2\theta_1(y) = 0\,, \tag{2.19}$$

$$\frac{d^2 C_0(y)}{dy^2} + d_0\frac{dC_0(y)}{dy^2} - d_1 C_0(y) = 0\,, \tag{2.20}$$

$$\frac{d^2 C_1(y)}{dy^2} + d_0\frac{dC_1(y)}{dy^2} - d_2 C_1(y) = 0\,, \tag{2.21}$$

The transformed boundary conditions (2.11) are

$$\begin{Bmatrix} u_0(0) = 0\,, & u_0(1) = 0\,, & u_1(0) = 0\,, & u_1(1) = 0 \\ \theta_0(0) = 0\,, & \theta_0(1) = 1\,, & \theta_1(0) = 0\,, & \theta_1(1) = 0 \\ C_0(0) = 0\,, & C_0(1) = 1\,, & C_1(0) = 0\,, & C_1(1) = 0 \end{Bmatrix} \tag{2.22}$$

The solutions of the eqs (2.13) - (2.18) the under boundary conditions (2.19) yield to

$$u(y,t) = \begin{bmatrix} \left\{B\sinh(m_1 y) + \dfrac{a_3\sin(b_2 y)}{(b_2^2 + m_1^2)\sin b_2} - \dfrac{a_4 A}{(n_1^2 - m_1^2)}(e^{n_1 y} - e^{-n_1 y})\right\} \\ + \varepsilon\exp(i\omega t)\left\{\dfrac{\lambda_1(\cosh m_2 - 1)}{m_2^2\sinh m_2}\sinh(m_2 y) - \dfrac{\lambda_1}{m_2^2}(\cosh(m_2 y) - 1)\right\} \end{bmatrix} \tag{2.23}$$

$$\theta(y) = \frac{\sin b_2 y}{\sin b_2} \tag{2.24}$$

$$C(y) = A(e^{n_1 y} - e^{-n_1 y}) \tag{2.25}$$

– **Skin friction**

$$\tau = \left[\frac{\partial u}{\partial y}\right] = \left[\begin{array}{c} \left\{\begin{array}{c} Bm_1\cosh(m_1 y) + \dfrac{a_3 b_2 \cos(b_2 y)}{(b_2^2 + m_1^2)\sin b_2} \\ -\dfrac{a_4 A n_1}{(n_1^2 - m_1^2)}(e^{n_1 y} + e^{-n_1 y}) \end{array}\right\} \\ +\varepsilon\exp(i\omega t)\left\{\begin{array}{c} \dfrac{\lambda_1(\cosh m_2 - 1)}{m_2 \sinh m_2}\cosh(m_2 y) \\ -\dfrac{\lambda_1}{m_2^2}(m_2\cosh(m_2 y) - 1) \end{array}\right\} \end{array}\right] \tag{2.26}$$

– **Nusselt Number**

$$Nu = \left[\frac{\partial\theta}{\partial y}\right] = \frac{b_2 \cos b_2 y}{\sin b_2} \tag{2.27}$$

– **Sherwood Number**

$$Sh = \left[\frac{\partial C}{\partial y}\right] = An_1(e^{n_1 y} + e^{-n_1 y}) \tag{2.28}$$

3. VALIDITY AND ACCURACY

To check the accuracy of the present nanofluid model, comparisons of the velocity and temperature of ZnO nanofluids have been conducted with published results obtained by Aaiza et al. (2015) and presented in Tables – 1 and 2. Very good agreement between the present and the previous results confirms the accuracy of the method used. The results obtained for velocity and temperature profiles through analytically have also been weighted up in the Tables – 1 and 2, respectively, which clearly reflects the convergence of the perturbation method. It has been seen that the increasing values of ϕ reduces the momentum and thermal boundary layer of ZnO nanofluids.

Table – 1: Comparison of velocity distribution with Aaiza et al. (2015) for ϕ in ZnO–water based Nanofluids at $\lambda = 1, \omega = 2, R = 2, Gr = 2, K = 0.01$:

	Aaiza et al. (2015) at Q = 0,Gm = 0			Present work at Q=2,Gm=2		
y	ϕ =0.01	ϕ =0.05	ϕ =0.09	ϕ=0.01	ϕ =0.05	ϕ =0.09
0.0	0	0	0	0	0	0
0.2	0.007568	0.006102	0.004402	0.00596	0.005589	0.00446
0.4	0.013975	0.0111024	0.007841	0.01228	0.01101	0.00842
0.6	0.017910	0.013637	0.009263	0.01880	0.015314	0.010843
0.8	0.016980	0.0115310	0.007302	0.022305	0.01509	0.009567
1.0	0	0	0	0	0	0

Table – 2: Comparison of temperature distribution with Aaiza et al. (2015) for ϕ in water based Nanofluids at $\psi = 0.81, R = 2, \kappa_f = 0.613, \kappa_s = 13$:

	Aaiza et al. (2015) at Q = 0			Present work at Q=5		
Y	ϕ =0.05	ϕ =0.1	ϕ =0.15	ϕ =0.05	ϕ =0.1	ϕ =0.15
0.0	0	0	0	0	0	0
0.2	0.36827	0.330702	0.305015	0.155128	0.14417	0.13627
0.4	0.68811	0.624609	0.58097	0.32071	0.30108	0.28685
0.6	0.917484	0.849022	0.80159	0.50792	0.48458	0.46750
0.8	1.02621	0.97897	0.94584	0.72937	0.71089	0.69719
1.0	1	1	1	1	1	1

4. RESULTS AND DISCUSSIONS

The effects of flow parameters such as the Magnetic Parameter (M), Radiation parameter (R), Porosity parameter (K), Grashof numbers (Gm, Gr), Chemical reaction (Kr), Suction (S), Schmidt number(Sc)on velocity, temperature, concentration, skin-friction, Nusselt number and Sherwood number have been studied analytically and presented graphically in Fig.1 to Fig.11 for cylindrical shaped ZnO nanoparticles. Default values of the parameters which have been used in graphical analyze for the effectiveness of the model are as follows: $\lambda = 1, t = 2, \omega = 2, R = 2, Gr = 2, Gm = 2, K = 0.01, Re = 2, Pe = 3.5, Kr = 0.05, S = 2, M = 2,$
$\sigma = 0.8, \gamma = 0.62, a = 13.5, b = 904.4, Q = 2.$

Table – 3: Constant a and b (Empirical shape factor)

Model	Platelet	Blade	Cylinder	Brick
a	37.1	14.6	13.5	1.9
b	612.6	123.3	904.4	471.4

Table – 4: Sphericity γ for different shapes nanoparticles:

Model	Platelet	Blade	Cylinder	Brick
γ	0.52	0.36	0.62	0.81

Table – 5: Thermo physical properties of water and nanoparticles:

Model	$\rho(kgm^{-3})$	$C_p(kg^{-1}K^{-1})$	$\kappa\ (wm^{-1}k^{-1})$	$\beta \times 10^{-5}\ (K^{-1})$
H_2O	997.1	4179	0.618	21
ZnO	5600	495.2	13	4.3

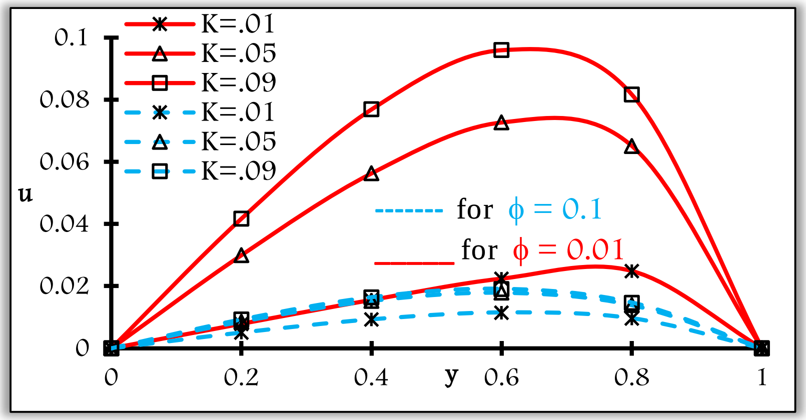

Figure 1: Velocity Distribution for K in ZnO-water based Nanofluid for ϕ =0.01 and ϕ =0.1

The nanofluids' velocity profiles are presented in Figure 1 for different estimations of the porosity parameter (K). Here velocity of the nanofluid is elevated for large values of K. In this figure ϕ =0.1 is dominated by ϕ =0.01 as velocity increases for small values of nanoparticles volume fraction (ϕ) and hence momentum boundary layer thickness depressed by ϕ =0.1. While momentum boundary layer thickness gradually increased by the higher porosity.

The velocity profiles (u) are plotted in Figure 2 for different estimations of nanoparticles volume fraction (ϕ) and Magnetic parameter (M). It is seen that velocity accelerates for small values of ϕ. Clearly the presence of Magnetic field is to diminish the velocity in the momentum boundary layer due to the fact that the utilization of the transverse magnetic field brings about an opposing kind of force called Lorentz force, like drag force that opposes the fluid flow which results in reducing the velocity of the nanofluid in the boundary layer. Moreover, higher MHD and nanoparticle volume fraction reduced the boundary layer thick ness.

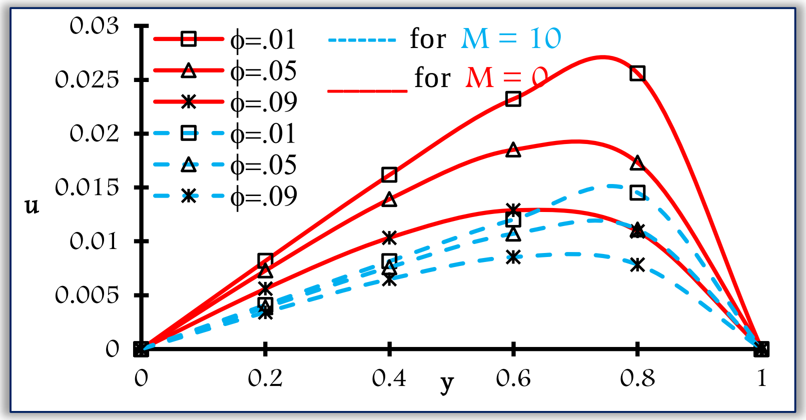

Figure 2: Velocity Distribution for ϕ in ZnO-water based Nanofluid for M=0 and M=10

Figure 3 depicts the velocity profiles for different values of Grashof Number (Gr) with M. It is clearly seen that for the both values of M, an increasing in Gr elevated the nanofluid velocity. Also is noticed that M=0.5 is followed by M=5, that means M retards the naonofluid motion.

The effect of heat generation parameter (Q) and radiation (R) in nanofluid velocity and temperature is presented in Figures 4 and 5. In the both Figures, with increasing Q, velocity and temperature profiles of the nanofluid decline this brings about diminishing the momentum and thermal boundary layer thickness with larger Q. It is observed that the velocity and temperature increase with increasing radiation parameter, and hence R=2 is followed by R=0.2 in both Figures.

Significantly, without heat generation (Q = 0) maximum heat fluctuations is observed for the higher R = 2 near y = 1, while θ becomes a linear function for the least R = 0.2 .

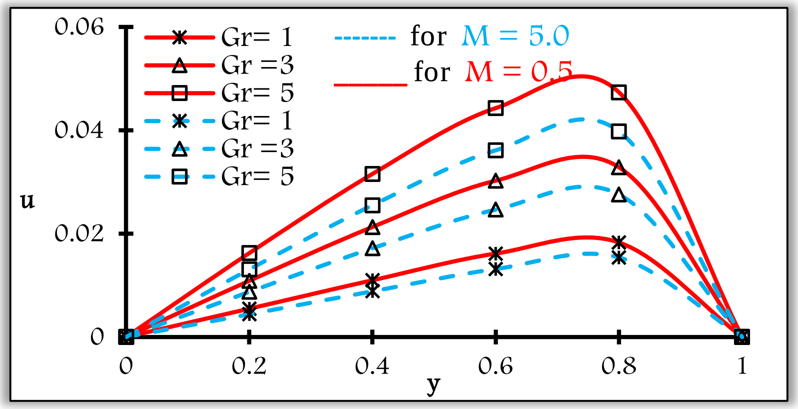

Figure 3: Velocity Distribution for Gr in ZnO-water based Nanofluid for M=0.5 and M=5

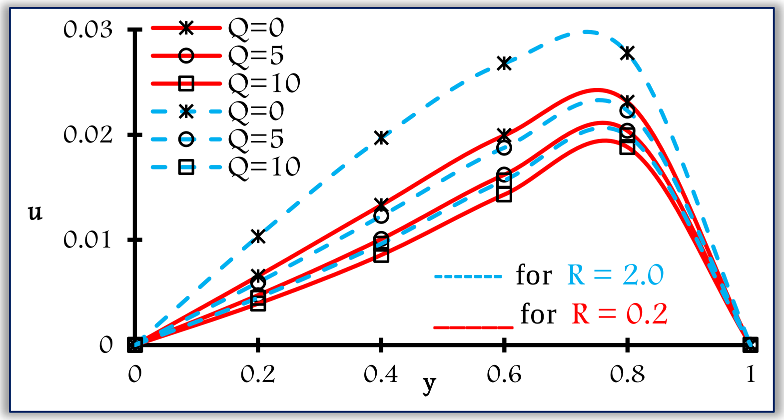

Figure 4: Velocity Distribution for Q in ZnO-water based Nanofluid for R=0.2 and R=2

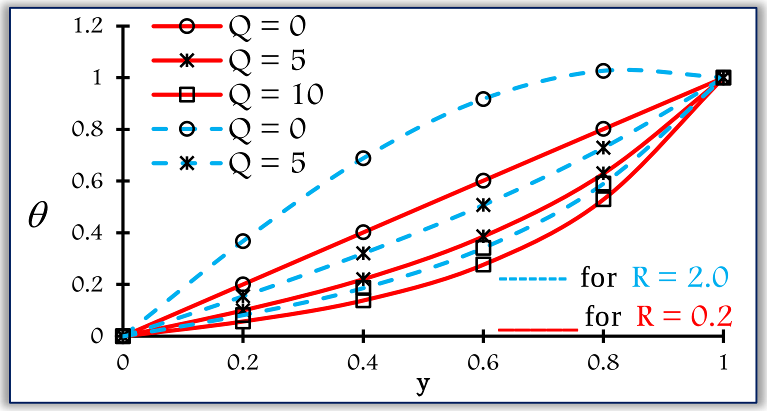

Figure 5: Temperature Distribution for Q in ZnO-water based Nanofluid for R=0.2 and R=2

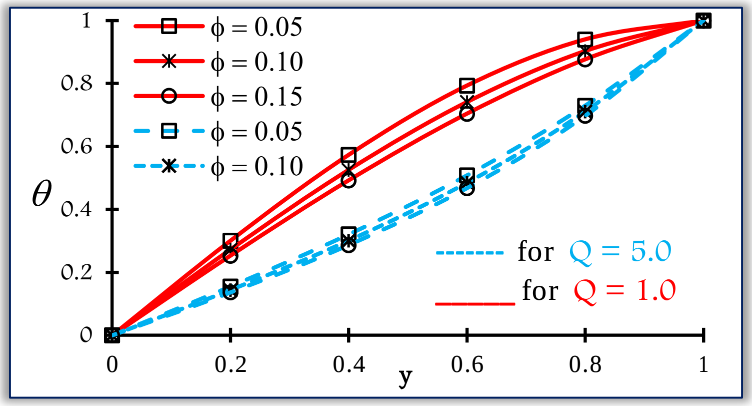

Figure 6: Temperature Distribution for ϕ in ZnO-water based Nanofluid for Q=1 and Q=5

Figure 6 is a graphical representation of different values of nanoparticles volume fraction (ϕ) and heat generation (Q) on temperature distribution. It is seen that temperature of ZnO diminishes for large values of ϕ and Q and hence the thermal boundary layer thickness becomes smaller. Moreover, the greater heat generation always suppresses the thermal boundary layer thickness. However, maximum θ is occurred near $y = 1$ for the least $Q = 1$ and this behaviour is opposite for the higher $Q = 5$.

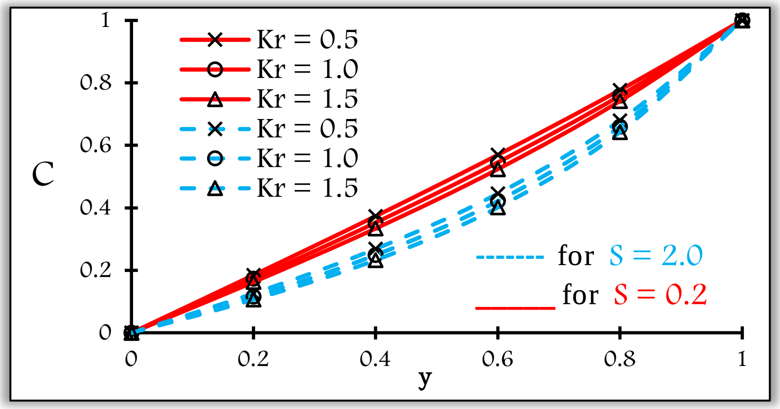

Figure 7: Concentration Distribution for Kr in S=0.2 and S=2

Figure 7 demonstrates the behavior of chemical reaction (Kr) and suction (S) on concentration profiles. It is marked that the concentration boundary layer is diminished by the effect of maximum suction parameter (S=2) and destructive chemical reaction (Kr = 1.5). The behavior of Kr and S reduces the species concentration in the channel of porous medium and hence S=2 is dominated by S=0.2 in a chemically reacting fluid.

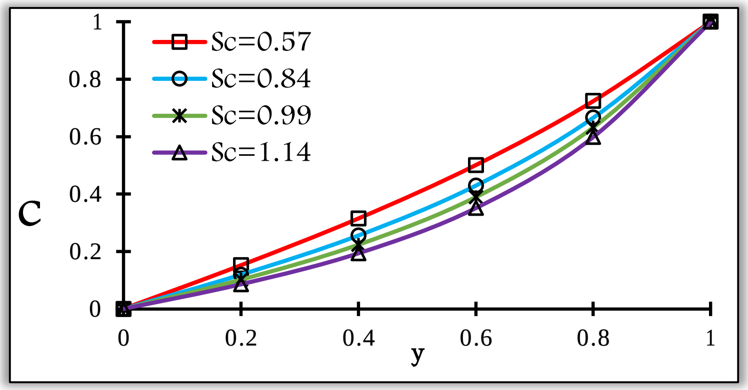

Fig.8: Concentration Distribution for Sc in air at 25º Celsius

The behavior of Sc on concentration profiles for air at the temperature of 25º Celsius is presented in Figure 8. An increase of Sc from Ammonia (Sc=0.57), Oxygen (Sc=0.84) through Methane (Sc=0.99) to Carbon dioxide (Sc=1.14) depress the species concentration boundary layer as heavy molecular diffusivity suppress the concentration profiles in boundary layer.

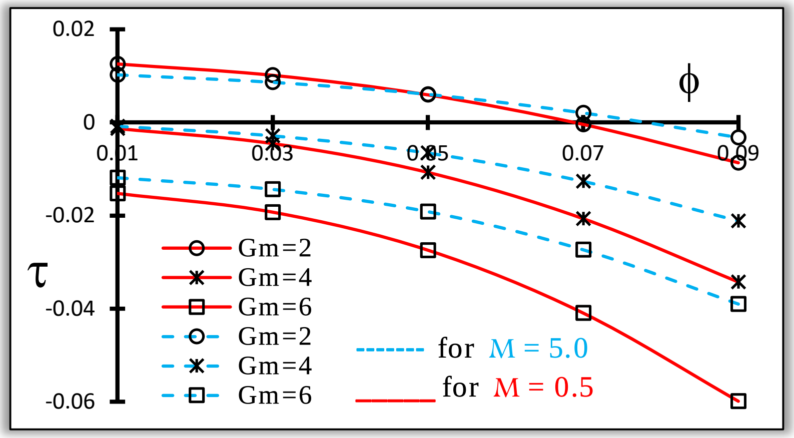

Figure 9: Skin friction for Gm in ZnO-water based Nanofluid for M=0.5 and M=5

In Figure 9, Skin friction profile for mass Grashof number (Gm) in ZnO-water based Nanofluid is plotted for two different M=0.5 and M=5 against nanoparticle volume fraction (ϕ). Skin friction profiles gradually diminishes, when Gm and ϕ increase. In presence of ZnO, the shear stresses become negative at the plate $y = 0$ for higher values of Gm=4, 6 and M=5. At ϕ =0.05 and Gm=2 a reverse behavior is observed for the shear stresses.

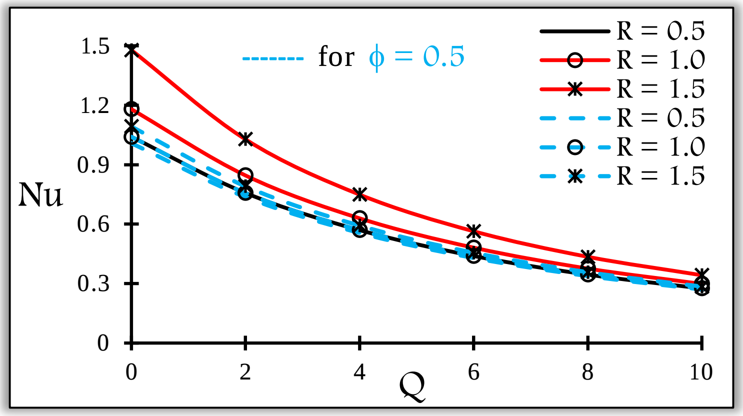

Figure 10: Rate of heat transfer at y=0 for Q and R in ZnO-water based Nanofluid when ϕ=0.01 and ϕ= 0.5

The effects of heat generation and radiation parameter on Nusselt number is displayed in Figure 10. Due to the bigger thermal conductivity of ZnO, the rate of heat transfer has dominant value at the lower $\phi = 0.01$ than the higher value $\phi = 0.5$. However, the thermal radiation (R) enhanced the rate of heat transfer, but this behaviour is reversed for the heat generation (Q).

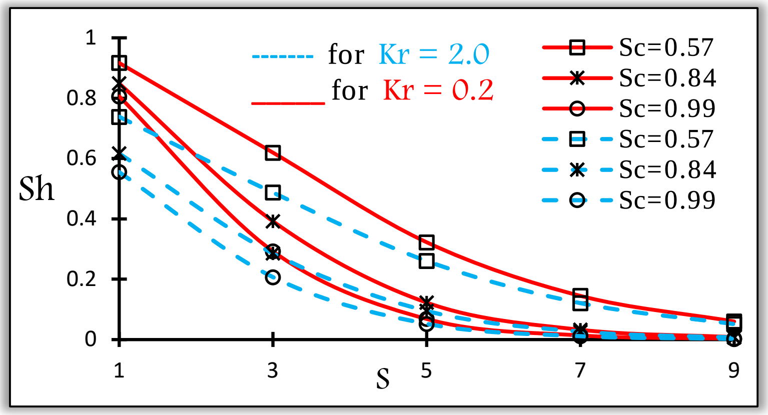

Figure 11: Sherwood number for Sc and Kr

In Figure 11 the effect of endothermic first order chemical reaction (Kr) and different values of Schmidt number (Sc) against suction (S) is presented for Sherwood number profile. Due to the cause of endothermic rate, the concentration is reduced throughout the channel and it is observed that Kr=2 is dominated by Kr=0.2. Sherwood number profiles strongly reduce with increasing Sc values. Also Sherwood number diminishes for greater values of suction parameter.

5. CONCLUSIONS

Impact of nanoparticle volume fraction of water based ZnO nanofluid in a chemically reacting fluid through a channel of porous medium with magnetic drag force and thermal radiation is investigated. During investigation of the results obtained through graphs and tables, few significant conclusions are mentioned below:

— The results obtained here are useful in engineering problems, particularly, in energy systems, rheology, material processing, lubrication and biomedical applications
— Due to Cylindrical shaped water based Zinc Oxide nanofluid, the velocity overshoot is observed in all the cases.
— The behaviour of nanoparticle volume fraction ϕ =0.01 is the most dominating agent in Zinc Oxide nanofluid over $\phi = 0.1$ for velocity, temperature and rate of heat transfer.
— In presence of water based ZnO nanofluid, porosity and natural convection enhanced the boundary layer thickness in the channel.
— Shear stresses at y=0 gradually become negative in presence of Gm, ϕ and M.

— Significantly, the rate of mass transfer at $y = 0$ is more dominant at $Kr = 0.2$ than $Kr = 2.0$ and reduces exponentially to zero with the effects of Sc and S;
— Higher radiation $R = 2$ plays a dominant agent over the lower radiation $R = 0.2$ on velocity and temperature of ZnO – nanofluid, while they are reduced by higher Q.
— Lower magnetic field $(M = 0)$ and heat generation $(Q = 1)$ boost the profiles of velocity and temperature of ZnO – nanofluid in comparison of higher M and Q, while ϕ reduces the thickness of boundary layer of u and θ.

Nomenclature:

$\bar{u}$	dimensional velocity component	κ_{nf}	thermal conductivity of nanofluid	ϕ	solid volume fraction of nanoparticles
$\bar{T}$	dimensional temperature of the nanofluid	β_{nf}	coefficient of thermal expansion of nanofluid	$\bar{K}_1$	dimensional permeability parameter
$\bar{C}$	dimensional concentration of the nanofluid	ρ_{nf}	density of the nanofluid	Q_0	dimensional additional heat source
u	non-dimensional velocity component along x-axis	μ_{nf}	viscosity of the nanofluid	Q	non- dimensional additional heat source
θ	non-dimensional temperature of the nanofluid	σ_{nf}	electric conductivity of nanofluid	Pe	Peclet Number
ψ	non-dimensional concentration of the nanofluid	$(\rho C_p)_{nf}$	heat capacitance of the nanofluid	K	non-dimensional permeability parameter
$\bar{T}_0$	temperature at $y = 0$	$(\rho\beta)_{nf}$	thermal expansion coefficient of the nanofluid	Re	Renolds Number
$\bar{C}_0$	concentration at $y = 0$	α_{nf}	thermal diffusivity of the nanofluid	S	suction$(S > 0)$, injection $(S < 0)$
$\bar{T}_w$	temperature of the wall	ρ_f	density of the base-fluid	M	magnetic parameter
$\bar{C}_w$	concentration of the wall	ρ_s	density of the nanoparticles	K_r	chemical reaction parameter
B_0	magnetic field strength	μ_f	viscosity of the base-fluid	Sc	Schmidt number
g	acceleration due to gravity	ρ_f	density of the base-fluid	Gr	thermal Grashof number
κ_f	thermal conductivity of base-fluid	ρ_s	density of the nanoparticles	Gm	mass Grashof number
κ_s	thermal conductivity of nanoparticles	$(\rho\beta)_f$	thermal expansion coefficient of the base-fluid	ε	reference constant due to perturbation
σ_f	electric conductivity of base-fluid	$(\rho\beta)_s$	thermal expansion coefficient of the nanoparticles	ω	angular velocity
t	time	$(\rho C_p)_f$	heat capacitance of the base-fluid	a, b	empirical Shape factor
γ	Sphericity	$(\rho C_p)_s$	heat capacitance of the nanoparticles		

Appendix:

$$
\left\{
\begin{array}{c}
\phi_1 = (1-\phi) + \phi\dfrac{\rho_s}{\rho_f}, \quad \phi_2 = 1 + a\phi + b\phi^2, \phi_3 = 1 + \dfrac{3(\sigma-1)\phi}{(\sigma+2)-(\sigma-1)\phi} \\
\phi_4 = (1-\phi) + \phi\dfrac{(\rho\beta)_s}{(\rho\beta)_f}, \quad \phi_5 = (1-\phi) + \phi\dfrac{(\rho C_p)_s}{(\rho C_p)_f}, \quad \lambda_1 = \dfrac{\lambda}{\phi_2}, \\
a_0 = \phi_1 Re, \quad m_0^2 = M^2 + \dfrac{\phi_2}{K}, \quad a_1 = \phi_4 Gr, \quad a_2 = \phi_4 Gm, \quad a_3 = \dfrac{a_1}{\phi_2}, a_4 = \dfrac{a_2}{\phi_2} \\
b_0^2 = \phi_5 Pe\dfrac{1}{\lambda_n}, \quad b_1^2 = \dfrac{R^2}{\lambda_n}, b_2^2 = b_1^2 - Q, b_3^2 = b_2^2 - b_0^2 i\omega, \quad m_1^2 = \dfrac{m_0^2}{\phi_2}, \quad m_2^2 = \dfrac{m_0^2 + a_0 i\omega}{\phi_2}, \\
d_0 = Sc.S, \quad d_1 = Sc.Kr, d_2 = Sc(i\omega + Kr), n_1 = \dfrac{d_0 + \sqrt{d_0^2 + 4d_1}}{2}, A = \dfrac{1}{e^{n_1} - e^{-n_1}}, \\
B = \dfrac{1}{\sinh m_1}\left\{\dfrac{a_4 A(e^{n_1} - e^{-n_1})}{(n_1^2 - m_1^2)} - \dfrac{a_3}{b_2^2 + m_1^2}\right\}
\end{array}
\right\}
$$

References

[1] S.U.S. Choi, Enhancing thermal conductivity of fluids with Nanoparticles, Developments and Applications of Non-Newtonian Flows, 231(66), 99–105 (1995).
[2] M. Sheikholeslami and A.J. Chamkha, Flow and convective heat transfer of a ferro-nanofluid in a double-sided lid-driven cavity with a wavy wall in the presence of a variable magnetic field, Numerical Heat Transfer, Part A: Applications, 69, 1186–1200 (2016).

[3] M., Hoghoughi, G., Mohebbi, R. and M. Sheremet, Nanoparticle migration and natural convection heat transfer of Cu-water nanofluid inside a porous undulant-wall enclosure using LTNE and two-phase model, Journal of Molecular Liquids, 261, 357–372 (2018).
[4] S. Reddy, P. Sreedevi, and A. J. Chamkha, MHD boundary layer flow, heat and mass transfer analysis over a rotating disk through porous medium saturated by Cu-water and Ag-water nanofluid with chemical reaction, Powder Technology, 307, 46-55 (2017).
[5] M. Sheikholeslami, T. Hayat and A. Alsaedi, MHD free convection of Al_2O_3–water nanofluid considering thermal radiation: A numerical study, Int. J. Heat and Mass Transfer, 96, 513–24 (2016).
[6] P.S. Reddy, P. Sreedevi and A.J. Chamkha, MHD boundary layer flow, heat and mass transfer analysis over a rotating disk through porous medium saturated by Cu-water and Ag-water nanofluid with chemical reaction, Powder Technology, 307(1), 46-55, 2017. https://doi.org/10.1016/j.powtec.2016.11.017.
[7] A. N. Al-Shamani, K. Sopian, H. Mohammed, S. Mat, M.H. Ruslan and A.M. Abed, Enhancement heat transfer characteristics in the channel with trapezoidal rib–groove using nanofluids, Case Studies in Thermal Engineering, 5, 48 –58 (2015).
[8] T. Hayat, M.B. Ashraf, S.A. Shehzad and A. Alsaedi, Mixed Convection Flow of Casson Nanofluid over a Stretching Sheet with Convectively Heated Chemical Reaction and Heat Source/Sink, Journal of Applied Fluid Mechanics, 8(4), 803-813 (2015).
[9] G. Aaiza, I. Khan and S. Shafie, energy transfer in mixed convection MHD flow of nanofluid containing different shapes of nanoparticles in a channel filled with saturated porous medium, Nanoscale Research Letters, 10, 490-503 (2015)
[10] S. Das, R. N. Jana and O. D. Makinde, Mixed convective magnetohydrodynamic flow in a vertical channel filled with nanofluids, Engineering Science and Technology, 18, 244 –255 (2015).
[11] W. Ibrahim and B. M. Shankar, MHD boundary layer flow and heat transfer of a nanofluid past a permeable stretching sheet with velocity, thermal and solutal slip boundary conditions, Computers & Fluids, 75, 1-10 (2013).
[12] A. J. Chamkha, S. Abbasbandy, A. M. Rashad and K. Vajravelu, Radiation effects on mixed convection about a cone embedded in a porous medium filled with a nanofluid, Meccanica, 48(2), 275–285 (2013).
[13] R.A. Mahdi, H.A. Mohammed, K.M. Munisamy, and N.H. Saeid, Review of convection heat transfer and fluid flow in porous media with nanofluid, Renew. Sustain. Energy Rev., 41, 715–734 (2015).
[14] M. Hassan and R. Ellahi, Convective heat flow of Nanofluid in a porous medium over wavy surface, Physics Letter A, 382(38), 2749-2753 (2018).
[15] A.K. Pandey and M. Kumar, The chemical reaction and thermal radiation effects on boundary layer flow of nanofluid over a wedge with viscous and Ohmic dissipation, St. Petersburg Polytechnical University Journal: Physics And Mathematics, 3(4), 322-332 (2017).
[16] C. Zhang, L. Zheng, X. Zhang and G. Chen, MHD flow and radiation heat transfer of nanofluids in porous media with variable surface heat flux and chemical reaction, Appl Math Comput., 39, 165-181 (2015).
[17] P.D. Prasad, R.V. Kumar, and S.V.K. Varma, Heat and mass transfer analysis for the MHD flow of nanofluid with radiation absorption, Ain Shams Engineering Journal, 9, 801-813 (2016).
[18] Md. Z. Akbar, Md. Ashraf, Md. F. Iqbal and K. Ali, Heat and mass transfer analysis of unsteady MHD nanofluid flow through a channel with moving porous walls and medium, AIP Advances 6, 045222 (2016); https://doi.org/10.1063/1.4945440 .2016
[19] P. Uikey and K. Vishwakarma, Review of Zinc Oxide (Zno) Nanoparticles Applications and Properties, Int. J. of Emerging Technology in Computer Science & Electronics, 21(2), 239-242 (2016).
[20] A.S. Dogonchi, M. Alizadeh and D.D. Ganji, Investigation of MHD Go-water nanofluid flow and heat transfer in a porous channel in the presence of thermal radiation effect, Advanced Powder Technology, 28(7), 1815-1825 (2017)
[21] E.V. Timofeeva, R. L. Jules and S. Dileep, Particle shape effect on thermophysical properties of alumina nanofluids, J. Appl. Phys., 106, 01430 (2009).
[22] R.L. Hamilton and O.K. Crosser, Thermal conductivity of heterogeneous two-component systems, J. Industrial & Engineering Chemistry Fundamentals, 1, 187–191 (1962).

ANNALS of Faculty Engineering Hunedoara – International Journal of Engineering
ISSN 1584 - 2665 (printed version); ISSN 2601 - 2332 (online); ISSN-L 1584 - 2665